J Radioanal Nucl Chem (2013) 295:167–177
DOI 10.1007/s10967-012-1891-y

Magnetic Th(IV)-ion imprinted polymers with salophen schiff base for separation and recognition of Th(IV)

F. F. He · H. Q. Wang · Y. Y. Wang · X. F Wang · H. S. Zhang · H. L. Li · J. H. Tang

Received: 21 February 2012 / Published online: 26 June 2012

Abstract A new complex of *N*,*N*′-bis(3-allyl salicylidene)*o*-phenylenediamine and thorium(IV) (Th(IV)) was synthesized and used as the functional monomer for a novel Th(IV) magnetic ion-imprinted polymer; this polymer was synthesized using a surface imprinting technique that included the modified magnetic Fe_3O_4 particle and used tetraethyl orthosilicate, 3-Aminopropyltriethoxysilane and maleic anhydride in the process. The magnetic polymer was characterized using FT-IR, and powder- and single crystal-XRD. The behavior of Th(IV) was investigated using batch experiments. At pH 4.5, the uptake capacity of this adsorbent and that of the non-imprinted polymer was 42.54 and 14.10 mg g^{-1}, respectively, and the relative selectivity coefficient values of the synthesized adsorbent for Th(IV)/La(III), Th(IV)/Ce(III), Th(IV)/Nd(III), and Th(IV)/U(VI) were 82.2, 93.1, 21.0 and 62.4 times greater than that of the non-imprinted matrix, respectively. In addition, the Th(IV) adsorption process using Fe_3O_4@-SiO_2-IIP follows pseudo-second-order reaction kinetics and the Langmuir adsorption isotherm. The thermodynamic parameters also suggest that the adsorption of Th(IV) onto Fe_3O_4@SiO_2-IIPs was a spontaneous and endothermic process.

Keywords Magnetic absorbent · Thorium ion · Imprinted polymers · Schiff base · Separation

F. F. He · H. Q. Wang (✉) · Y. Y. Wang · X. F Wang · H. S. Zhang · H. L. Li · J. H. Tang
School of Chemistry and Chemical Engineering, University of South China, 28 Changsheng West Road, Hengyang 421001, Hunan, People's Republic of China
e-mail: hqwang2009cn@yahoo.com.cn

Introduction

Thorium (Th) is widely distributed in the environment and is present at low levels in water, soil, rocks, plants and animals. It is an important element not only in industrial applications but also in energy and environmental issues. Because of the extensive usage of Th for various industrial purposes and also because of its toxicity and radioactivity, pre-concentration or separation of Th in environmental and biological samples is significant [1, 2]. Numerous methods have been developed to pre-concentrate or separate Th from environmental and biological sources, including co-precipitation [3], liquid–liquid extraction [4, 5], solid-phase extraction (SPE) [6–8], extraction chromatography [9, 10], ion exchange [11], and membrane separation [12].

The SPE method uses ion surface imprinted polymers (IIP), which can avoid the grinding and sieving that can occur in other methods. IIP, the best used method for pre-concentration or separation of trace metals, also has high selectivity, good mass transfer, and fast binding kinetics [13–15]. And the IIP was used as the adsorbent of SPE and applied to the extraction of thorium ion by more and more researchers. Sibel and his fellows [16] prepared the Th(IV)-imprinted beads with *N*-methacryloyl-(L)-glutamic acid (MAGA) as the complexing monomer by suspension polymerization. Qun He et al. [17] synthesized Th(IV)-imprinted polymers (IIPs) by surface imprinting technology with a new functional monomer *N*-(*o*-carboxyphenyl)maleamic acid (CPMA) on the surface of silica gel. The Th(IV)-imprinted chitosan-phthalate particles, which were synthesized by the complexing monomer and epichlorohydrin as crosslinking agent, were reported by Birlik et al. [15]. We also reported the preparation and characterization of the Th(IV)-imprinted material based on the surface of silica gel with methacrylic acid (MAA) as a functional monomer [18].

Magnetic materials, which support surface imprinted polymers, have been widely used in the pre-concentration and separation process because they are simple to use [19–21], but not found in reports of the Th(IV)-imprinted polymer.

During the ion imprinting process, a functional ligand determines selectivity and affinity for the target ion. Furthermore, it is trend for IIP to choose ion coordinate with ligand. Salophen schiff bases strongly coordinate to metals ions [22–24], and were found to possess high affinity to form complexes with Th(IV) [25, 26].

Thus, to further our previous research [27, 28], the aim of this study was to synthesize a new magnetic surface Th(IV)-imprinted sorbent, based on a novel complex of *N*,*N*'-bis(3-allylsalicylidene)*o*-phenylenediamine (BASPDA) with Th(IV) as the functional monomer and template, and using a modified magnetic Fe_3O_4 particle as its support. In this manner, we have developed a new method to pre-concentrate and separate trace Th(IV). We describe, in this article, the interaction of the sorbent with the Th ion and its corresponding mechanism of adsorption. As the paragraph said, the magnetic.

Materials and methods

Materials

Azobisisobutyronitrile (AIBN, 98 %), 3-Aminopropyltriethoxysilane (APTES), maleic anhydride, salicylaldehyde, *o*-phenylenediamine, allylchloride, 2-propanol, Tetraethyl orthosilicate (TEOS), Arsenazo III, Chlorophosphonazo(CPA)-III, iron(II) chloride tetrahydrate ($FeCl_2{\cdot}4H_2O$), iron(III) chloride hexahydrate ($FeCl_3{\cdot}6H_2O$) were obtained from Aladdin (Shanghai, China). Ethylene glycol dimethacrylate (EGDMA) was purchased from EHSY (Shanghai, China), and $Th(NO_3)_4{\cdot}4H_2O$ (SP) was purchased from Hengrui New Materials Co. Ltd. (Chengdu, Sichuan).

Unless otherwise stated, reagents of analytical purity were used for all experiments and double-distilled water (DDW) was used throughout. Standard labware and glassware were washed with 10 % HNO_3 and rinsed with DDW. Arsenazo III solution was prepared by dissolving an appropriate amount of reagent in DDW. The pH adjustments were made with 0.1 mol L^{-1} HCl or 0.1 mol L^{-1} NH_4OH. Standard stock solutions (1 mg mL^{-1}) of Th(IV), U(VI), Ce(III), La(III) and Nd(III) were prepared by dissolving appropriate amounts of nitrate salts in DDW containing 1.0 mol L^{-1} HNO_3 and were further diluted daily prior to use.

Apparatus

A Perkin-Elmer Lambda 45 UV–Visible spectrometer (USA) was used for determination of the metal ion concentration. IR Spectra (4,000–400 cm^{-1}) were recorded on IR Prestige-21 (Shimadzu, Japan) using KBr pellets. ^1H NMR spectra were recorded with a Bruker Avance III 500 MHz spectrometer with $CDCl_3$ as the solvent. Powder XRD patterns of the particles were collected on a Rigaku D/max-RA powder diffraction meter (Rigaku, Japan), and the single-crystal XRD was collected on a Bruker APXII CCD diffractometer using graphite monochromated Mo Kα radiation ($\lambda = 0.71073$ Å). A pHs-l0C digital pH meter (Pengshun Scientific Instruments Research, Shanghai, China) was used for the pH adjustments.

Synthesis of *N*,*N*'-bis(3-allylsalicylidene)*o*-phenylenediamine (BASPDA)

The mechanism of BASPDA synthesis is presented in Scheme 1. The mixture of KOH (80 mmol, 4.48 g) and salicylaldehyde (80 mmol, 9.76 g) was stirred at room temperature for 30 min. Then, 6.88 g allylchloride was added to this solution, and the mixture was refluxed for 17 h. The mixture was then allowed to cool gradually to room temperature and filtered. When the solvent was removed, an oily liquid was obtained; the oily liquid was then mixed with ether and water (at a ratio of 1:1), and the organic phase was washed sequentially with 10 % NaOH solution, water and brine, and then dried with anhydrous Na_2SO_4. Finally, the crude 2-(vinyloxy)benzaldehyde was obtained by removing the solvent [29]. Then, the 2-(vinyloxy)benzaldehyde was incubated for 24 h at 190 °C under a nitrogen atmosphere. After cooling the mixture slightly, the light-yellow 2-hydroxy-3-vinylbenzaldehyde was obtained by distilling the mixture under a vacuum (bp, 142–145 °C, 18 mmHg) [30].

Sequentially, 50 mL ethanol, followed by the synthesized 2-hydroxy-3-vinylbenzaldehyde (3.24 g) and then o-phenylenediamine (1.09 g) were added to a three-neck flask, and the mixture was refluxed for 2 h. After cooling the mixture to 0 °C, yellow solids were obtained by filtering the mixture. When the yellow compound was recrystallized using absolute ethanol, yellow crystals were obtained; these yellow crystals were BASPDA and they were analyzed by IR and ^1H NMR. IR analysis results (cm^{-1}) are as follows: 3,452 (O–H), 2,902 (C–H), 1,637 (C=N), 1,573 (C=C), 906 (=C–H), 746 (C–H). The ^1H NMR($CDCl_3$) δ analysis results are as follows: 13.09 (s, 1H,–OH), 8.58 (s, 2H,–CH=N), 6.86–7.32 (m, 10H, Ar–H), 6.04 (2H, m,–CH=), 5.00 (4H, d, $=CH_2$), 3.41 (4H, d, $–CH_2–$).

Preparation of $Th(BASPDA)_2$ complexes

The $Th(BASPDA)_2$ complexes were formed through a chemical reaction as previously described [25]. Briefly,

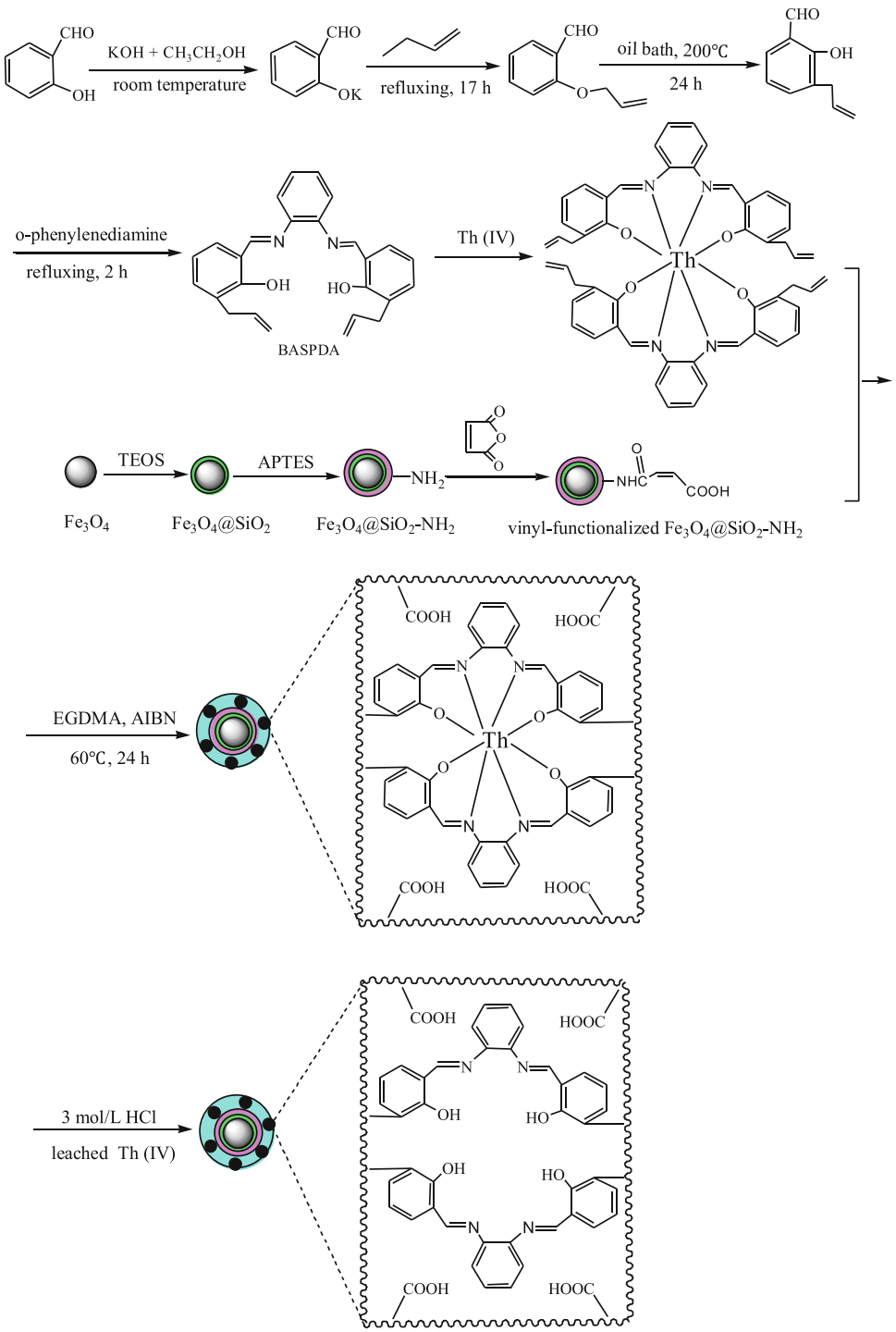

Scheme 1 A schematic representation of the mechanism of synthesis of the functional monomer and preparation of the Th(IV)-imprinted polymers

BASPDA (1.58 g), $Th(NO_3)_4{\cdot}4H_2O$ (1.10 g) and absolute ethanol (30 mL) were refluxed for 1 h, and the $Th(BASPDA)_2$ complexes were obtained by filtering the mixture. When the yellow compound was re-crystallized using DMF and anhydrous ethanol (1:1), 2.08 g of yellow crystals were obtained. These yellow crystals were analyzed using IR, and the results (cm^{-1}) are as follows: 420 (Th–O), 530 (Th–N), 1,637 (C=N), 1,581 (C=C).

Preparation of vinyl modified Fe_3O_4

Preparation of Fe_3O_4@SiO_2

Fe_3O_4 was prepared as previously described [31], and SiO_2 was used to prepare Fe_3O_4@SiO_2 as was also previously described [32, 33]. Briefly, 5.00 g Fe_3O_4 was dissolved in 250 mL 2-propyl alcohol and 20 mL DDW by sonication

for 15 min, followed by the sequential addition of 20 mL ammonia solution and 33.3 mL TEOS. The resulting product was collected by an external magnetic field after the reaction had continued for 12 h at room temperature with continuous stirring, followed by six rinses with purified water, and thorough drying.

Preparation of amino-functionalized Fe_3O_4@SiO_2 (Fe_3O_4@SiO_2–NH_2)

As previously described [34], 4.00 g Fe_3O_4@SiO_2 and 100 mL of toluene were added to a 250 mL three-necked flask and then ultrasonically dispersed for 15 min. APTES (8 mL) was then added into the flask, and the mixture was refluxed at 110 °C with continuous stirring for 12 h under a flow of nitrogen. After the mixture was allowed to cool gradually to room temperature, the resulting amino-functionalized Fe_3O_4@SiO_2 was collected by filtering the mixture, washing it several times with ethanol and acetone, and then drying it.

Preparation of vinyl-functionalized Fe_3O_4@SiO_2–NH_2

As previously described [24], a solution of maleic anhydride (2.50 g) in DMF (25 mL) was added to the three neck flask containing Fe_3O_4@SiO_2–NH_2 (4.00 g) and DMF (25 mL). After the mixture was stirred for 24 h at room temperature, the resulting products were collected by filtration, washed sequentially with DMF, anhydrous ethanol and anhydrous ether, and dried under a vacuum at room temperature. Vinyl-functionalized magnetic particles were obtained.

Synthesis of magnetic surface Th(IV)-imprinted (Fe_3O_4@SiO_2-IIPs) and non-imprinted polymers (Fe_3O_4@SiO_2-NIPs)

The mechanism of synthesis for the magnetic surface Th(IV)-imprinted polymers (Fe_3O_4@SiO_2-IIPs) is presented in Scheme 1. $Th(BASPDA)_2$ complexes (1.02 g) dissolved in DMF (25 mL), vinyl-functionalized magnetic particles (2.00 g), AIBN (0.15 g) and EGDMA (6 mL) were added to a three neck flask. Then, the oxygen was removed by sonication for 15 min and nitrogen was bubbled through the mixture for 25 min. The mixture was stirred and heated under nitrogen at 60 °C for 24 h. After the mixture was cooled to room temperature, the products were collected by filtration, washed with methanol/water/DMF (1:1:1) and treated with 3 mol L^{-1} HCl for 24 h to remove Th(IV) from the polymers. The final products were rinsed with DDW several times until all the acid was removed, and the exiguous granules were removed by rinsing with acetone, then drying under a vacuum at 70 °C for 24 h. In this manner, the magnetic surface Th(IV)-imprinted polymers were obtained. Non-imprinted polymers (Fe_3O_4@SiO_2-NIPs) were also prepared using the same method, except that the $Th(NO_3)_4{\cdot}4H_2O$ was omitted.

Adsorption experiments

A series of metal ion standard solutions (Th(IV), Th(IV)/U(VI), Th(IV)/La(III), Th(IV)/Ce(III), or Th(IV)/Nd(III)) were transferred into a 25 mL color comparison tube, and the pH values were adjusted to the desired value with 0.1 mol L^{-1} HCl or 0.1 mol L^{-1} $NH_3{\cdot}H_2O$. After the volume was adjusted to 25 mL with DDW, Fe_3O_4@SiO_2-IIPs or Fe_3O_4@SiO_2-NIPs polymers (30 mg) were added, and the mixture was shaken vigorously for 30 min. Then the mixture was centrifuged (3,000 rpm for 10 min), and the concentrations of Th ions in the solutions were determined by spectrophotometry, using Arsenazo-III (0.05 %, w/v) as a chromogenic agent in a 3 mol L^{-1} HNO_3 medium at a wavelength of 660 nm. The concentrations of U(IV) (at 658 nm) and Ce(III)–La(III) (at 652 nm) were determined in buffer solutions of chloroacetic acid-sodium chloroacetate of pH 2.5 and 2.8, respectively, while the concentration of Nd(III) was determined at a wavelength of 670 nm using Chlorophosphonazo(CPA)-III as a indicator agent, and the concentrations were compared to a reagent blank that was used as a reference for all samples. All the experiments were carried out in triplicate. The amount of adsorption, the removal efficiency, the distribution coefficient K_d (mL g^{-1}), the selectivity coefficient k, and the relative selectivity coefficient k' were calculated by Eqs. 1–5, respectively.

$$Q = \frac{C_0 - C_e}{W} \times V \tag{1}$$

$$E = \frac{C_0 - C_e}{C_0} \times 100\,\% \tag{2}$$

$$K_d = \left(\frac{C_0 - C_e}{C_e}\right)\frac{V}{W} \tag{3}$$

$$k = \frac{K_{d(Th)}}{K_{d(M)}} \tag{4}$$

$$K' = \frac{k_{(IIP)}}{k_{(NIP)}} \tag{5}$$

where Q represents the amount of Th(IV) adsorbed on the polymer (mg g^{-1}), E represents the percent (%) removal efficiency, C_0 and C_e represent the initial and equilibrium concentrations, respectively, of the given metal ions in solution (μg mL^{-1}), W is the amount of polymer (mg), and V is the volume of metal ion solutions (mL). $K_{d(Th)}$ and $K_{d(M)}$ represent the distribution coefficients of Th(IV) and M ions, respectively. $k_{(IIP)}$ and $k_{(NIP)}$ represent the

selectivity coefficient of Fe_3O_4@SiO_2-IIPs and Fe_3O_4@-SiO_2-NIPs, respectively.

Desorption procedure

Magnetic Th(IV)-imprinted polymers (50 mg) that had adsorbed Th(IV) ions were packed into a glass column (120 mm × 5.5 mm i.d.). The ends of the column were plugged with a small portion of glass wool to prevent loss of the sorbents during sample loading. Then, the stoichiometric HCl solutions were passed through the column by a peristaltic pump at a flow rate of 1.0 mL min^{-1} until no Th(IV) ion was detected in the eluent.

Results and discussion

Characteristics of the adsorbent

The FT-IR spectra

FT-IR was used to characterize Fe_3O_4@SiO_2, Fe_3O_4@-SiO_2–NH_2, vinyl-functionalized Fe_3O_4@SiO_2–NH_2, Fe_3O_4@SiO_2-IIPs containing Th(IV), and Fe_3O_4@SiO_2-NIPs (Fig. 1). For all six particles absorption peaks at 586 cm^{-1} were observed, corresponding to the Fe–O vibration from the magnetite phase. As presented in Fig. 1a, the peaks at 401, 814, 957 and 1,084 cm^{-1} were attributed to the stretching of SiO_2 [27, 34]. The presence of adsorbed water is reflected by the –OH vibration at 1,630 and 3,441 cm^{-1}, which suggests that the SiO_2 has been successfully immobilized on Fe_3O_4 surface [35]. Successful amino-functionalization of Fe_3O_4@SiO_2 was also verified by the absorption peak at 1,409 cm^{-1} and 3,439 cm^{-1} (Fig. 1b), attributed to the stretching and bending vibrations of amino groups. Moreover, there were absorption peaks from methylene groups of Fe_3O_4@SiO_2–NH_2 at 2,951 and 2,981 cm^{-1}. The peaks at 1,720 and 1,544 cm^{-1} represent the stretching vibration of C=O and C=C, respectively (Fig. 1c).

The spectra presented in Fig. 1d–f have similar characteristics. Comparing the spectrum in Fig. 1c with those in Fig. 1d–f, the vibration intensity of the methylene groups on Fe_3O_4@SiO_2-IIPs and Fe_3O_4@SiO_2-NIPs are greater than that on Fe_3O_4@SiO_2–NH_2. In addition, the spectrum in Fig. 1d–f had the following unique peaks: 1,500–1,600 cm^{-1} and 600–900 cm^{-1} (benzene ring); 1,635–1,641 cm^{-1} (C=N) (Fig. 1d–f); 420 cm^{-1} (Th–O stretching vibrations, Fig. 1d [36]; and 530 cm^{-1} (Th–N stretching vibrations, Fig. 1d) [37]. There were absorption peaks of the Th–O and Th–N groups of Th(IV) attached to Fe_3O_4@SiO_2-IIPs at 420 cm^{-1} and 530 cm^{-1}, respectively, but these peaks could not be seen in the IR spectra of Fe_3O_4@SiO_2-IIPs and Fe_3O_4@SiO_2-NIPs. These results suggested that the Th(IV) ion-imprinted magnetic polymer with BASPDA as a functional monomer was formed, and that the Th(IV) ion had been removed completely.

Powder and single-crystal XRD analysis

The crystalline structures of the synthesized magnetic particles were studied with XRD. There were six characteristic peaks observed for Fe_3O_4 (2θ = 30.3°, 35.7°, 43.6°, 53.9°, 57.4°, and 63.0°) (Fig. 2). These six peaks correspond to the six crystal faces of Fe_3O_4 and are (220), (311), (400), (422), (511) and (440), respectively [38]. In Fig. 2b–f, the same set of characteristic peaks as for the Fe_3O_4@SiO_2, Fe_3O_4@-SiO_2–NH_2, vinyl-functionalized Fe_3O_4@SiO_2, Fe_3O_4@-SiO_2-NIP, and Fe_3O_4@SiO_2-IIP were observed. In addition, the six peaks of the Fe_3O_4 (Fig. 2d–f) were observed for the synthesized vinyl-functionalized Fe_3O_4@SiO_2, Fe_3O_4@-SiO_2- NIP and Fe_3O_4@SiO_2-IIP, but the intensity of the peaks was slightly decreased in these latter 3 compounds. Thus, it was concluded that the modified magnetic particles

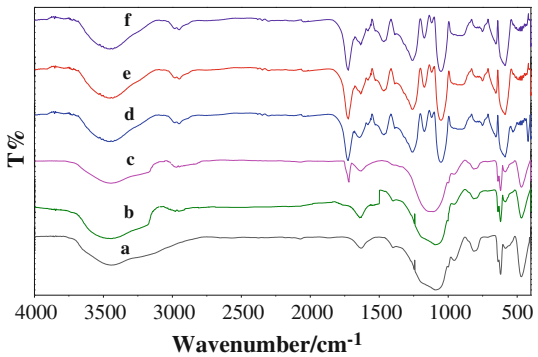

Fig. 1 FT-IR spectra: (*a*) Fe_3O_4@SiO_2; (*b*) Fe_3O_4@SiO_2–NH_2; (*c*) vinyl-functionalized Fe_3O_4@SiO_2–NH_2; (*d*) Th(IV) Fe_3O_4@-SiO_2-IIP containing Th(IV); (*e*) Fe_3O_4@SiO_2-IIPs with Th(IV) removed; (*f*) Fe_3O_4@SiO_2–NIPs

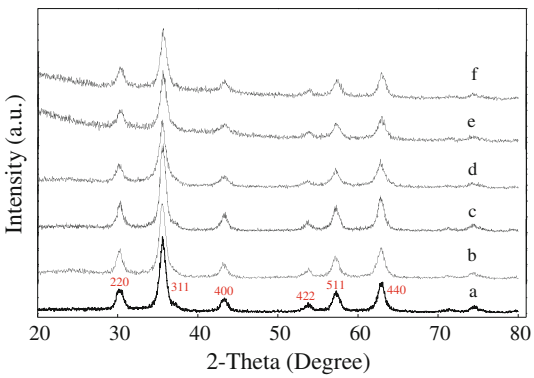

Fig. 2 XRD patterns of (*a*) Fe_3O_4, (*b*) Fe_3O_4@SiO_2, (*c*) Fe_3O_4@SiO_2–NH_2, (*d*) vinyl-functionalized Fe_3O_4@SiO_2–NH_2, (*e*) Fe_3O_4@SiO_2-NIPs and (*f*) Fe_3O_4@SiO_2-IIPs

and the imprinted polymer were in a spinel structure, and that the crystalline structure of the magnetite was essentially maintained; it was also concluded that SiO_2, NH_2 and BASPDA were successfully immobilized on the surface of Fe_3O_4.

The crystal structure of the compound $Th(BASPDA)_2$ was determined, and X-ray intensity data were recorded on a Bruker APXII CCD diffraction meter using graphite monochromated Mo Kα radiation ($\lambda = 0.71073$ Å). A total of 47,678 reflections were measured, of which 15,646 were unique ($R_{int} = 0.032$) in the range of $1.14° < \theta < 25.00°$ (h, −17 to 19; k, −20 to 20; l, −22 to 20), and 12434 observed reflections with $I > 2\sigma(I)$ were used in the refinement on F^2. The structure was solved by direct methods with the SHELXS-97 program. All of the non-H atoms were refined anisotropically by a full-matrix least-squares analysis to give the final $R = 0.0314$ and $wR = 0.0914$ ($w = 1/[\sigma^2 (F_o^2) + (0.0477P)^2 + 3.7353P]$, where $P = (F_o^2 + 2F_c^2)/3$ with $(\Delta/\sigma)_{max} = 0.004$ and $S = 1.043$ by using the SHELXL program. The hydrogen atoms were located using a difference Fourier map and refined isotropically. The details of the crystal structure were published elsewhere, and the cell structure of the crystal is shown in Fig. 3.

Affect of pH

The effect of pH was investigated in the pH range of 2.0 to 6.0 using the batch procedure with 10 mL of Th(IV) (1.0 μg mL^{-1}) (Fig. 4). The adsorption percentage of the Th(IV) increased as the pH increased from pH 2.0 to 4.5, and there was a further increase between pH 4.5 and pH 6.0. At pH ≤ 2.5, the adsorption percentage was very low. From the structure of the compound $Th(BASPDA)_2$, it was found that

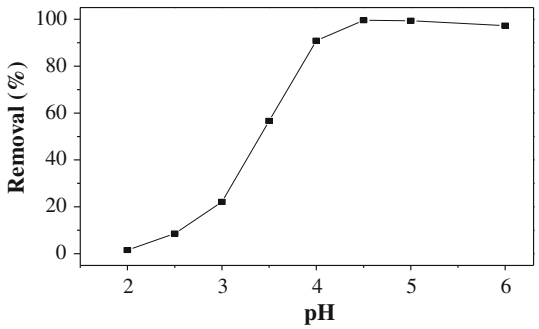

Fig. 4 The effect of pH on adsorption of Th(IV) on the Th(IV)-imprinted polymers; 10 mL Th(IV) 1.0 μg mL^{-1}; temperature 25 °C

the interactions of Th(IV) with Fe_3O_4@SiO_2-IIPs were the coordination of the Th(IV) with the N and O atoms on the BASPDA groups in the polymers. There were also competitive reactions between the N and O in the sorbent and the metal ions and hydrogen ions in the solution. At pH ≤ 2.5, most of N and O of the BASPDA was protonated; by increasing the pH, the ratio of the free BASPDA group to the protonated BASPDA group increases, resulting in a greater chance of interaction between BASPDA and Th(IV); at pH ≥ 7, the Th(IV) ion is easily hydrolyzed and precipitated. At pH = 4.5, the adsorption rate of Th(IV) was 99.55 %, and thus pH 4.5 was picked as the optimum pH level for subsequent experiments.

Adsorption kinetics

The adsorption rate of the imprinted polymer for Th(IV) ions was determined to be between 1 and 40 min. In the experiment, 30 mg of the polymer was added to 25 mL of 10 μg mL^{-1} Th(IV) aqueous solution after adjusting the

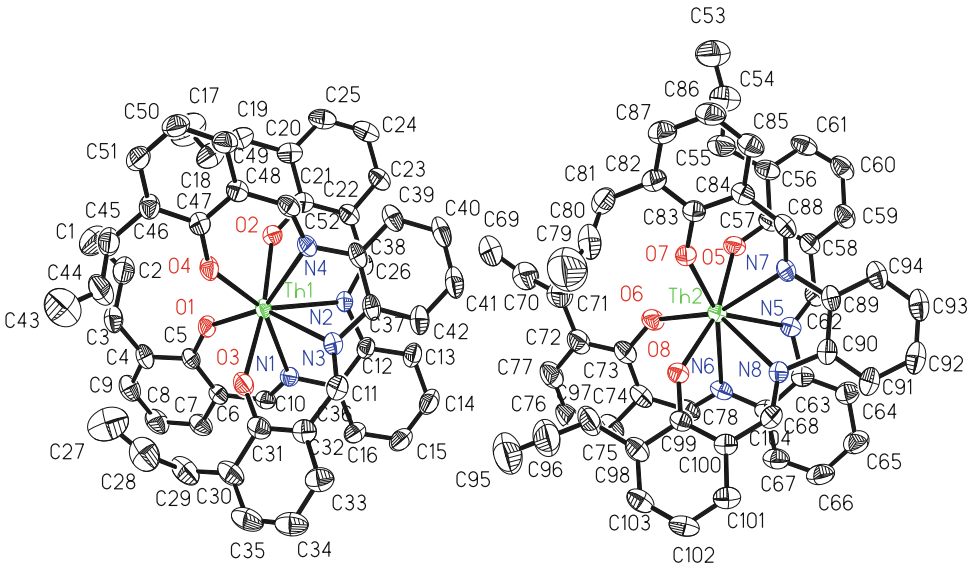

Fig. 3 The shell structure of $Th(BASPDA)_2$ crystal

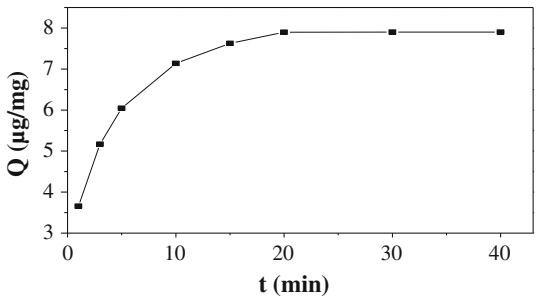

Fig. 5 The adsorption rate of Th(IV) on Th(IV)-imprinted adsorbent. pH 4.5; 25 mL Th(IV) 10 μg mL^{-1}; temperature 25 °C

pH to 4.5; the equilibration time was approximately 20 min (Fig. 5).

In order to investigate the mechanism of adsorption kinetics, two different kinetic models were tested to interpret the data obtained from the batch experiments [39].

The pseudo-first-order equation is:

$$\ln(q_e - q_t) = \ln q_e - k_1 t \quad (6)$$

The pseudo-second-order equation is:

$$\frac{t}{q_t} = \frac{1}{k_2 q_e^2} + \left(\frac{1}{q_e}\right) t \quad (7)$$

where q_e (mg g^{-1}) and q_t (mg g^{-1}) are the adsorption amount at equilibrium and the time t (min), respectively. The q_e values were calculated from the intercept of the $\ln(q_e - q_t)$ versus t plot. The slope of t/q_t versus t is defined as the theoretical q_e(cal) value of pseudo-first-order and pseudo-second-order model, respectively. k_1 (min^{-1}) and k_2 (mg g^{-1} min^{-1}) are pseudo-first-order and pseudo-second-order rate constants of adsorption, respectively.

The pseudo-first-order kinetic model indicates that the rate of adsorption site occupation is proportional to the number of unoccupied sites; the pseudo-second-order kinetic model assumes that the chemical reaction mechanisms [40] and also the adsorption rate are controlled by chemical adsorption through sharing or exchange of electrons between the adsorbate and adsorbent [41]. The correlation coefficients (R^2) of the pseudo-first-order kinetic model and pseudo-second-order kinetic model for adsorption of Th(IV) ions onto the Fe_3O_4@SiO_2-IIPs were 0.8462, 0.9994, respectively (Fig. 6). Also, the q_e value estimated from pseudo-second-order kinetic model was closer to the experimental value than that of pseudo-first-order kinetic model (Table 1). These results demonstrated that the pseudo-second-order adsorption mechanism was the best-fit model to describe the adsorption behavior of Th(IV) onto the synthesized imprinted particles, and that this adsorption mechanism was a chemical coordination process.

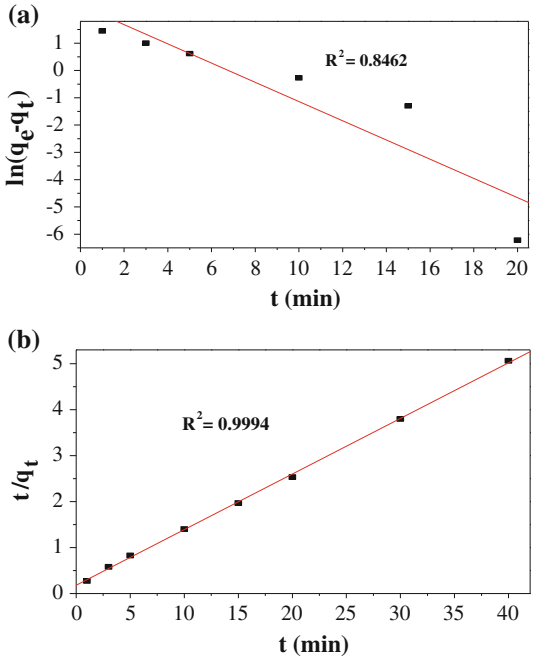

Fig. 6 **a** pseudo-first-order kinetic model, **b** pseudo-second-order kinetic model

Adsorption isotherm

The adsorption capacity of Fe_3O_4@SiO_2-IIPs and Fe_3O_4@SiO_2-NIPs for Th(IV) was investigated by batch experiments in the concentration range of 5 μg mL^{-1} to 90 μg mL^{-1}. The amount of Th(IV) ions adsorbed per unit mass of the Fe_3O_4@SiO_2-IIPs and Fe_3O_4@SiO_2-NIPs increases with the increasing initial concentration of Th(IV), until a saturation value was achieved (Fig. 7). The maximum adsorption capacities of the imprinted and non-imprinted particles were 42.54 and 14.10 mg g^{-1}, respectively. Compared with Fe_3O_4@SiO_2-NIPs, the adsorption capacity of Th(IV) on Fe_3O_4@SiO_2-IIPs was almost three times that of Fe_3O_4@SiO_2-NIPs, which indicates that the cavities created after removal of Th(IV) in Fe_3O_4@SiO_2-IIP are complementary to the imprint ion in size, shape, coordination geometries and chemical functionality, whereas in Fe_3O_4@SiO_2-NIPs there is a random distribution of ligand functionalities in the polymeric network.

The equilibrium experimental data were analyzed using the Langmuir and the Freundlich isotherms.

The Langmuir isotherm is represented by the following expression [42]:

$$\frac{C_e}{Q_e} = \frac{1}{Q_{max} b} + \frac{C_e}{Q_{max}} \quad (8)$$

The Langmuir dimensionless separation factor R_L is expressed as follows:

Table 1 Kinetic parameters of the pseudo-order rate equation for Th(IV) adsorption onto Th(IV)-IIP

Experimental q_e (mg g^{-1})	Pseudo-first-order rate equation			Pseudo-second-order rate equation		
	k_1 (min^{-1})	q_e (mg g^{-1})	R^2	k_2 ((g mg^{-1}) min^{-1})	q_e (mg g^{-1})	R^2
7.90	0.3521	10.83	0.8642	0.08163	8.26	0.9994

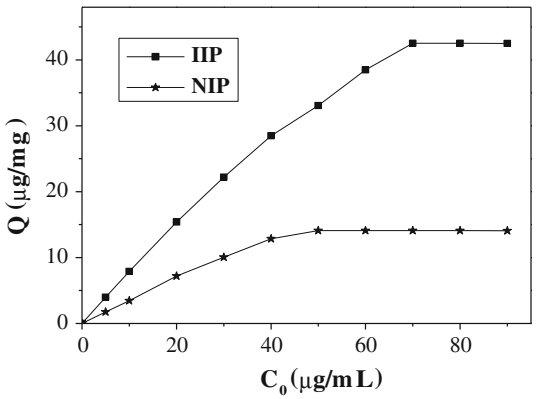

Fig. 7 The effect of Th(IV) initial concentration (C_0) on the adsorption quantity (Q) of Th(IV)-IIP and NIP adsorbent, pH 4.5; sample volume 25 mL; temperature 25 °C

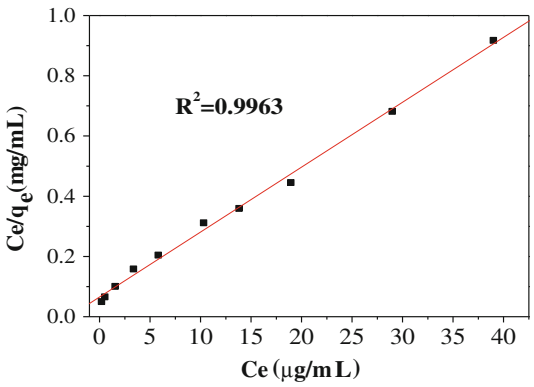

Fig. 8 The Langmuir isotherm for the adsorption of Th(IV) on the Th(IV)-imprinted, polymers; pH 4.5; temperature 25 °C

$$R_L = \frac{1}{1 + bC_0} \tag{9}$$

The Freundlich isotherm equation is [43]:

$$\ln Q_e = \ln K_F + \left(\frac{1}{n}\right) \ln C_e \tag{10}$$

Where Q_e (mg g^{-1}) is the amount of Th(IV) adsorbed at equilibrium, C_e (μg mL^{-1}) is the equilibrium concentration of Th(IV) in the solution, Q_{max} is the maximum adsorption quantity; b (L mg^{-1}) is the Langmuir constant; and K_F and n are the Freundlich constants, which indicate the adsorption capacity and the adsorption intensity, respectively, in the Freundlich isotherm equation.

The Langmuir isotherm is a fixed monolayer adsorption onto a surface with a finite number of identical sites. The Freundlich isotherm is an empirical equation based on adsorption onto a heterogeneous surface. The Langmuir linear equation ($C_e/Q_e = 0.06549 + 0.02155C_e$, $R^2 = 0.9963$) and Freundlich isotherm equation ($\ln Q_e = 2.3728 + 0.4519 \ln C_e$, $R^2 = 0.9561$) for the adsorption of Th(IV) were obtained from experimental data (Figs. 8, 9). From the value of correlation coefficients (R^2), it was concluded that the Langmuir isotherm is a better fit to our data and best describes the adsorption isotherm in our experimental results. The values of R_L (Table 2), which were all between 0 and 1, indicate that favorable adsorption conditions were present in this process. Furthermore, the calculated value of Q_{max} (46.40 mg g^{-1}) from the Langmuir equation was comparable

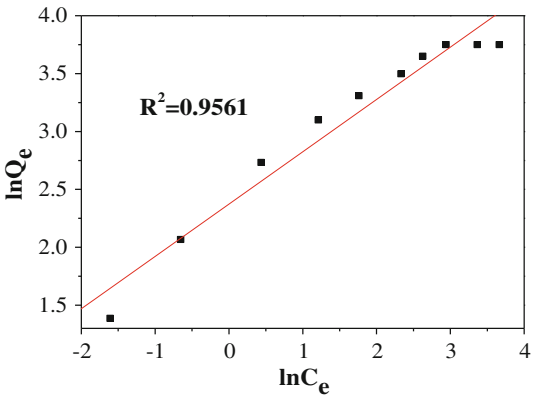

Fig. 9 The Freundlich isotherm for the adsorption of Th(IV) on the Th(IV)-imprinted, polymers; pH 4.5; temperature 25 °C

to the value (42.54 mg g^{-1}) obtained in our experiments, indicating that the process involves a monolayer adsorption and that Th(IV) was adsorbed onto the surface of the synthesized imprinted particles.

Uptake thermodynamics

In this research, the thermodynamic parameters for the adsorption of Th(IV) onto the Fe_3O_4@SiO_2-IIP were studied in the temperature range of 298.15 – 318.15 K. The thermodynamic parameters can be determined using the following equations:

Table 2 R_L values in the Langmuir isotherm of Th(IV)-IIP

C_0 (μg mL^{-1})	R_L
5	0.3780
10	0.2330
20	0.1319
30	0.09197
40	0.07060
50	0.05729
60	0.04820
70	0.04160
80	0.03659
90	0.03266

$$\Delta G^\circ = \Delta H^\circ - T\Delta S^\circ \quad (11)$$

$$\Delta G^\circ = -RT \ln K \quad (12)$$

$$\ln K = \frac{\Delta S^\circ}{R} - \frac{\Delta H^\circ}{RT} \quad (13)$$

$$K = \frac{q_e}{C_e} \quad (14)$$

where K is equilibrium constant, T (K) is the temperature, and R is the gas constant; and ΔS° (kJ mol^{-1} K^{-1}), ΔH (kJ mol^{-1}) and ΔG° (kJ mol^{-1}) are the standard entropy change, enthalpy and Gibbs free energy, respectively.

The linear equation representing the thermodynamic parameters is $\ln K = 0.0382 - 10.588/T$, with the slope represented by $-\Delta H^\circ/R$ and the intercept value described by $\Delta S^\circ/R$ (Fig. 10). The values for ΔH°, ΔS° and ΔG° are presented in Table 3. The positive ΔH° values suggest that the adsorption reaction was an endothermic reaction, and the positive ΔS° values indicate an increase in the randomness of the adsorption process in the experimental system (Table 3). The ΔG° values were obtained using Eq. 11 (Table 3), and the negative ΔG° values indicate the spontaneous nature of Th(IV) adsorption.

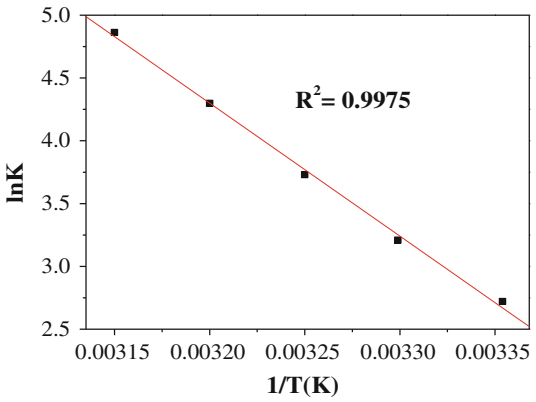

Fig. 10 The effect of temperature on the adsorption of Th(IV) on the Th(IV)-imprinted polymers; Th(IV) 10 μg mL^{-1}; pH 4.5

Adsorption selectivity

The competitive adsorption of Th(IV)/U(VI), Th(IV)/La(III), Th(IV)/Ce(III) and Th(IV)/Nd(III) from these combinations of ions (25 mL) was also investigated using a batch process because these ions often coexist in minerals or products, or have a similar ionic radius or the same ionic charge. The distribution ratio (K_d) values of Th(IV) in the Th(IV)-Fe_3O_4@SiO_2-IIP adsorbent was greater than that of the other metals (Table 4). The selectivity coefficient (k) for Th(IV)/U(VI), Th(IV)/La(III), Th(IV)/Ce(III) and Th(IV)/Nd(III) was 71.1, 649.2, 595.8 and 96.6, respectively. Also, the k of Fe_3O_4@SiO_2-IIP was 21 times to 93 times greater than that of Fe_3O_4@SiO_2-NIPs; this difference is likely due to the random distribution of ligand functionalities in the polymeric network of Fe_3O_4@SiO_2-NIPs, whereas this random distribution was not observed for Fe_3O_4@SiO_2-IIP. For Fe_3O_4@SiO_2-IIP, the cavities created after removal of the template were complementary to the size, shape and coordination geometries of the imprinted ion. The results described in this section show that the Th(IV)-imprinted adsorbent has a high selectivity for Th(IV) and that it Th(IV) is adsorbed even in the presence of La(III), Ce(III), Nd(III), and U(VI).

Desorption and regeneration

The uptake ratio onto the imprinted adsorbent is low below a pH of 2.5, as described above, which suggests that the adsorbed Th(IV) can be released into an acidic solution. Thus, the desorption of the adsorbed Th(IV) and regeneration of the polymer were tested in a desorption procedure conducted using different concentrations (0.1 to 2.5 mol L^{-1}), volumes (2 to 8 mL) and flow rates (0.5 to 6 mL min^{-1}) of HCl solutions. The results indicated that 1.0 mol L^{-1} HCl (5 mL) is sufficient for quantitative recovery of Th(IV) using a flow rate of 1.0 mL min^{-1}. The successive adsorption–desorption processes indicated that

Table 3 Thermodynamic parameters for the adsorption of Th(IV)-IIP

C_0 (μg mL^{-1})	ΔH° (KJ mol^{-1})	ΔS° (KJ mol^{-1} K^{-1})	ΔG°(KJ mol^{-1})				
			298.15 K	303.15 K	308.15 K	313.15 K	318.15 K
10	88.028	0.317	−6.486	−8.071	−9.656	−11.241	−12.826

Table 4 Competitive adsorption of different ions by Th(IV)-IIP and NIP sorbent (initial concentrations of metal ions: 10 μg mL^{-1}; sorbent 30 mg; temperature 25 °C)

Metal ions	K_d(IIP)	K_d(NIP)	K(IIP)	K(NIP)	k′
Th(IV)	15192.3	586.0	–	–	–
La(III)	23.4	74.0	649.2	7.9	82.2
Ce(III)	26.5	91.6	595.8	6.4	93.1
Nd(III)	157.2	128.7	96.6	4.6	21.0
U(VI)	213.8	514.0	71.1	1.14	62.4

Table 5 Comparisons of Th(IV-imprinted material with the results from different references

Th(IV)-imprinted material	pH	Q_{max} (mg g^{-1})	Repeated	Reference
Imprinted polymer with CPMA on silica gel	3	35.9	–	[17]
Th(IV)-IIP with MAA on silica gel	3	33.2	10	[18]
Th(IV)-imprinted chitosan-phthalate	3	61.25	5	[15]
Poly(MAGA-EDMA)	2–4	40.44	7	[16]
Material with salophen on magnetic particle	4.5	42.54	9	Present work

the uptake capacity of the Fe_3O_4@SiO_2-IIPs for Th(IV) was only reduced by approximately 5 % after nine repetitions under the optimal conditions. These results demonstrate that the Fe_3O_4@SiO_2-IIP can be used recovered and reused.

The comparisons of Th(IV-imprinted material with the results from different references were given in Table 5. The results from the table 5 show that the prepared sorbent gives better Q_{max} and repeated times.

Conclusions

This research has described a novel magnetic Th(IV)-imprinted polymer based on a new complex of the schiff base *N*,*N*′-bis(3-allyl salicylidene)*o*-phenylenediamine, with Th(IV) as the functional monomer. The template for this novel polymer was prepared successfully using surface imprinting technology. The imprinted polymers demonstrated acceptable characteristics, such as high affinity, selectivity and adsorption capacity, good reusability, and fast process kinetics for Th(IV). The adsorption behavior of Th(IV) was best described by a pseudo-second-order kinetic model, and the adsorption mechanism was a chemical coordination process. A Langmuir isotherm best described the experimental data and indicated a monolayer formation of Th(IV) ions at the surface of the sorbent. In addition, the thermodynamic studies indicated that the adsorption of Th(IV) was an endothermic and spontaneous process.

Acknowledgments This work was financially supported by the National Natural Science Foundation of China (No. 11175080) and by the Nature Science Fund of the Hunan Province (No. 10JJ6025).

References

1. Shtangeeva I, Ayrault S, Jain J (2005) Thorium uptake by wheat at different stages of plant growth. J. Environ Radioact 81:283–293
2. Rao TP, Metilda P, Gladis JM (2006) Preconcentration techniques for uranium(VI) and thorium(IV) prior to analytical determination—an overview. Talanta 68:1047–1064
3. Aydin FA, Soylak M (2007) A novel multi-element coprecipitation technique for separation and enrichment of metal ions in environmental samples. Talanta 73:134–141
4. Bayyari MA, Nazal MK, Khalili FI (2010) The effect of ionic strength on the extraction of thorium(IV) from perchlorate solution by didodecylphosphoric acid (HDDPA). Arab J Chem 3:115–119
5. Sharma JN, Ruhela R, Harindaran KN, Mishra SL, Tangri SK, Suri AK (2008) Separation studies of uranium and thorium using tetra(2-ethylhexyl) diglycolamide (TEHDGA) as an extractant. J Radioanal Nucl Chem 278:173–177
6. Hosseini MS, Hosseini BA (2010) Selective extraction of Th(IV) over U(VI) and other co-existing ions using eosin B-impregnated Amberlite IRA-410 resin beads. J Radioanal Nucl Chem 283:23–30
7. Krishina PG, Gladis JM, Rao KS, Rao TP, Naidu GRK (2005) Synthesis of xanthate functionalized silica gel and its application for the preconcentration and separation of uranium(VI) from inorganic components. J Radioanal Nucl Chem 266:251–257
8. Ayata S, Merdivan M (2010) *p-tert*-Butylcalix[8]arene loaded silica gel for preconcentration of uranium(VI) via solid phase extraction. J Radioanal Nucl Chem 283:603–607
9. Gopalkrishnan V, Dhami PS, Ramanujam A, Balaramakrishna MV, Murali MS, Mathur JN, Iyer RH, Bauri AK, Banerji A (1995) Extraction and extraction chromatographic separation of minor actinides from sulphate bearing high level waste solutions using CMPO. J Radioanal Nucl Chem 191:279–289
10. Naik PW, Dhami PS, Misra SK, Jambunathan U, Mathur JN (2003) Use of organophosphorus extractants impregnated on silica gel for the extraction chromatographic separation of minor actinides from high level waste solutions. J Radioanal Nucl Chem 257:327–332
11. Lee SH, Rosa JL, Gastaud J, Povinec PP (2005) The development of sequential separation methods for the analysis of actinides in sediments and biological materials using anion-exchange resins and extraction chromatography. J Radioanal Nucl Chem 263:419–425
12. Rastegarzadeh S, Pourreza N, Saeedi I (2010) An optical chemical sensor for thorium (IV) determination based on thorin. J Hazard Mater 173:110–114
13. Poole CF (2003) New trends in solid-phase extraction. Trends Anal Chem 22:362–373
14. Ghaedi M, Ahmadi F, Tavakoli Z, Montazerozohori M, Khanmohammadi A, Soylak M (2008) Three modified activated carbons by different ligands for the solid phase extraction of copper and lead. J Hazard Mater 152:1248–1255
15. Birlik E, Büyüktiryaki S, Ersöz A, Say R, Denizli A (2006) Selective separation of thorium using ion imprinted chitosan-

phthalate particles via solid phase extraction. Sep Sci Technol 41:3109–3121
16. Sibel B, Rıdvan S, Arzu E, Ebru B, Adil D (2005) Elective preconcentration of thorium in the presence of UO_2^{2+}, Ce^{3+} and La^{3+} using Th(IV)-imprinted polymer. Talanta 67:640–645
17. He Q, Chang XJ, Wu Q, Huang XP, Hu Z, Zhai YH (2007) Synthesis and applications of surface-grafted Th(IV)-imprinted polymers for selective solid-phase extraction of thorium(IV). Anal Chim Acta 605:192–197
18. Lin CR, Wang HQ, Wang YY, Zhou L, Liang J (2011) Selective preconcentration of trace thorium from aqueous solutions with Th(IV)-imprinted polymers prepared by a surface-grafted technique. Int J Environ Anal Chem 90:1050–1061
19. Ren YM, Zhang ML, Zhao D (2008) Synthesis and properties of magnetic Cu(II) ion imprinted composite adsorbent for selective removal of copper. Desalination 228:135–149
20. Li H, Bi S, Liu L, Dong W, Wang X (2011) Separation and accumulation of Cu(II), Zn(II) and Cr(VI) from aqueous solution by magnetic chitosan modified with diethylenetriamine. Desalination 278:397–404
21. Singh S, Barick KC, Bahadur D (2011) Surface engineered magnetic nanoparticles for removal of toxic metal ions and bacterial pathogens. J Hazard Mater 192:1539–1547
22. Tobiasz A, Walas S, Trzewik B, Grzybek P, Zaitz MM, Gawin M, Mrowiec H (2009) Cu(II)-imprinted styrene–divinylbenzene beads as a new sorbent for flow injection-flame atomic absorption determination of copper. Microchem J 93:87–92
23. Gupta KC, Abdulkadir HK, Chand S (2003) Synthesis of polymer anchored N,N′-bis(3-allyl salicylidene)*o*-phenylenediamine cobalt(II) Schiff base complex and its catalytic activity for decomposition of hydrogen peroxide. J Mol Catal A: Chem 202: 253–268
24. Amarasekara AS, Oki AR, McNeal I, Uzoezie U (2007) One-pot synthesis of cobalt-salen catalyst immobilized in silica by sol–gel process and applications in selective oxidations of alkanes and alkenes. Catal Commun 8:1132–1136
25. Hill RJ, Rickard CEF (1978) Complexes of thorium(IV) and uranium(IV) with some schiff base. J Inorg Nucl Chem 40: 793–797
26. Hill RJ, Rickard CEF, White HE (1981) The preparation of some complexes of Th(IV) and U(IV) with tetradentate Schiff base. J Inorg Nucl Chem 43:721–726
27. Lin CR, Wang HQ, Wang YY, Cheng ZQ (2010) Selective solid-phase extraction of trace thorium(IV) using surface-grafted Th(IV)-imprinted polymers with pyrazole derivative. Talanta 81:30–36
28. Cheng ZQ, Wang HQ, Wang YY, He FF, Zhang HS, Yang SQ (2011) Synthesis and characterization of an ion-imprinted polymer for selective solid phase extraction of thorium(IV). Microchim Acta 173:423–431
29. Khalil NSAM (2010) Efficient synthesis of novel 1,2,4-triazole fused acyclic and 21–28 membered macrocyclic and/or lariat macrocyclic oxaazathia crown compounds with potential antimicrobial activity. Eur J Med Chem 45:5265–5277
30. Claisen L, Eisleb O (1914) About transformations of phenyl allyl ethers into isomericallylphenols "Über die umlagerung von phenolallylät- hem in die isomeren allylphenole". Liebigs Ann 401:21–119
31. Li L, He XW, Chen LX, Zhang YK (2009) Preparation of novel bovine hemoglobin surface-imprinted polystyrene nanoparticles with magnetic susceptibility. Sci China Ser B Chem 52: 1402–1411
32. Wang X, Wang LY, He XW, Zhang YK, Chen LX (2009) A molecularly imprinted polymer-coated nanocomposite of magnetic nanoparticles for estrone recognition. Talanta 78:327–332
33. Luo XB, Luo SL, Zhan YC, Shu HY, Huang YN, Tu XM (2011) Novel Cu(II) magnetic ion imprinted materials prepared by surface imprinted technique combined with a sol–gel process. J Hazard Mater 192:949–955
34. Wang JH, Zheng SR, Shao Y, Liu JL, Xu ZY, Zhu DQ (2010) Amino-functionalized Fe_3O_4@SiO_2 core–shell magnetic nanomaterial as a novel adsorbent for aqueous heavy metals removal. J Colloid Interface Sci 349:293–299
35. Li Y, Li X, Chu J, Dong CK, Qi JY, Yuan YX (2010) Synthesis of core-shell magnetic molecular imprinted polymer by the surface RAFT polymerization for the fast and selective removal of endocrine disrupting chemicals from aqueous solutions. Environ Pollut 15:2317–2323
36. Nakamoto K (1986) Infrared and Raman spectroscopy of inorganic and coordination compounds, 4th edn. Wiley, New York
37. Reddy BN, Avaji PG, Badami PS, Patil SA (2008) Synthesis, characterization and fluorescence studies of Th(IV) complexes of Schiff bases derived from 2,6-diformyl-4-methyl phenol and 3-substituted-4-amino-5-mercapto-1,2,4-triazoles. J Coord Chem 61:1827–1838
38. Zhao YG, Shen HY, Pan SD, Hu MQ (2010) Synthesis, characterization and properties of ethylenediamine-functionalized Fe_3O_4 magnetic polymers for removal of Cr(VI) in waste water. J Hazard Mater 182:295–302
39. Sarin V, Pant KK (2006) Removal of chromium from industrial waste by using eucalyptus bark. Bioresour Technol 97:15–20
40. Iftikhar AR, Bhatti HN, Hanifa MA, Nadeem R (2009) Kinetic and thermodynamic aspects of Cu(II) and Cr(III) removal from aqueous solutions using rose waste biomass. J Hazard Mater 161:941–947
41. Özacara M, Sengilb IA, Türkmenler HJ (2008) Equilibrium and kinetic data, and adsorption mechanism for adsorption of lead onto valonia tannin resin. Chem Eng J 143:32–42
42. Demirbas E, Dizge N, Sulak MT, Kobya M (2009) Adsorption kinetics and equilibrium of copper from aqueous solutions using hazelnut shell activated carbon. Chem Eng J 148:480–487
43. Mezenner NY, Bensmaili A (2009) Kinetics and thermodynamic study of phosphate adsorption on iron hydroxide-eggshell waste. Chem Eng J 147:87–96